View Online / Journal Homepage / Table of Contents for this issue
Dynamic Article Links

Nanoscale

Cite this: *Nanoscale*, 2012, **4**, 3427

www.rsc.org/nanoscale

PAPER

Functional hybrid nickel nanostructures as recyclable SERS substrates: detection of explosives and biowarfare agents†

P. R. Sajanlal and T. Pradeep*

Received 7th March 2012, Accepted 14th March 2012
DOI: 10.1039/c2nr30557g

We present the synthesis of highly anisotropic nickel nanowires (NWs) and large area, free-standing carpets extending over cm^2 area by simple solution phase chemistry. The materials can be post-synthetically manipulated to produce hybrid tubes, wires, and carpets by galvanic exchange reactions with Au^{3+}, Ag^{+}, Pt^{2+}, and Pd^{2+}. All of these structures, especially the hybrid carpets and tubes, have been prepared in bulk and are surface enhanced Raman scattering (SERS) active substrates. Molecules of relevance such as dipicolinic acid (constituting 5–15% of the dry weight of bacterial spores of *Bacillus anthracis*), dinitrotoluene, hexahydro-1,3,5-triazine (RDX), and trinitrotoluene at nanomolar concentrations have been detected. An enhancement factor of ~10^{10} was observed for the Ni–Au nanocarpet. The reusability of the Ni–Au nanocarpet for SERS applications was tested 5 times without affecting the sensitivity. The reusability and sensitivity over large area have been demonstrated by Raman microscopy. Our method provides an easy and cost effective way to produce recyclable, large area, SERS active substrates with high sensitivity and reproducibility which can overcome the limitation of one-time use of traditional SERS substrates.

1. Introduction

Detection of trace amounts of explosives and chemical warfare agents is an important task in view of national security and defense. Potentially harmful materials such as disease causing bacterial spores, viruses, and toxins have to be identified at low concentrations quickly and accurately for the safety and well-being of the population. Though various detection techniques are available, systematic efforts have been ongoing to develop better analytical techniques to detect a multitude of hazardous materials in a cost-effective, rapid, and reliable manner. Anisotropic micro-/nanomaterials with well-defined physiochemical properties are of great interest to materials chemists in view of their morphology-, size-, and crystallinity-dependent intrinsic properties as well as attractive applications in the fields of catalysis, sensing, electronics, and bio-related applications.[1–3]

Surface enhanced Raman scattering (SERS)[4–10] is a phenomenon, exhibited by certain nanoparticles (NPs), which enables the rapid detection of molecules down to single molecule level, under ambient conditions. Highly anisotropic NPs such as triangles,[11,12] stars,[13] flowers,[4] *etc.*[4–9,11,14] are well-known for their excellent SERS activity and related applications.[15] Nanoparticle assemblies such as superlattices[16] also show similar enhancement, enabling them for sensing applications.[17] Theoretical predictions of field enhancement around various anisotropic nanostructures have been reported.[13,18,19] However, cost-effective production of a robust, reusable, large-area, and homogeneous SERS substrate with high sensitivity and reproducibility still remains an important issue. In view of making appropriate and affordable SERS substrates, synthesizing SERS active nanomaterials by making a thin coating of Au or Ag on prefabricated, cheap substrates gained popularity.[20,21] A periodic array of SERS active nanostructures can also be fabricated over a large area by nanosphere lithography techniques.[22] Most of these techniques have the major disadvantage of being very time consuming with high production costs. Solution based synthesis of most of the anisotropic nanomaterials requires various surfactants such as cetyltrimethylammonium bromide (CTAB) and sodium dodecyl sulfate (SDS) and polymers such as poly(*N*-vinyl-2-pyrrolidone) (PVP) and polyamines. The presence of such organic coating may reduce the efficiency and sensitivity of these NPs towards SERS activity.

The galvanic displacement reaction[23–28] is an easy way to make SERS active nanomaterials from a pre-fabricated NPs template. The galvanic displacement reaction has advantages over the other methods in synthesizing nanostructures since no surfactant or coordinating molecules are involved in the synthesis which can yield clean surfaces, and is an important attribute for surface enhanced spectroscopies. Here, we report the synthesis of thorny nickel nanowires (NWs) and nanocarpets (NCs) *via* a simple

---

DST Unit of Nanoscience (DST UNS), Department of Chemistry, Indian Institute of Technology Madras, Chennai 600 036, India. E-mail: pradeep@iitm.ac.in; Fax: +91-44 2257-0545

† Electronic supplementary information (ESI) available: SEM and EADX data of various materials such as Ni NC and NWs and their hybrid forms, SEM image of branched Ni NWs, XPS spectra of O 1s of various nanomaterials, Raman data showing higher detection limit and reusability of Ni–Au NCs. See DOI: 10.1039/c2nr30557g

chemical reduction route and their subsequent use as sacrificial templates for making highly SERS active, hybrid anisotropic materials such as Au–Ni NCs, NWs and nanotubes through the galvanic displacement reaction. Nickel NPs are very good candidates to use as sacrificial templates for making SERS active noble metal nanomaterials, as Ni is relatively cheap and has lower reduction potential (0.25 V for Ni^{2+}/Ni (*vs.* standard hydrogen electrode (SHE))) than noble metal ions (0.99 V for $AuCl_4^-/Au$, 0.76 V for $PtCl_4^{2-}/Pt$, and 0.59 V for $PdCl_4^{2-}/Pd$). Such hybrid materials show enhanced oxidation-resistance and stability, which make them useful for certain biological applications, catalysis and SERS.[29–31] Various other nanosystems like Ni–Pd nanotubes, Ni–Pt and Ni–Ag NWs were also made to demonstrate the viability of our method to make various hybrid nanomaterials. Reusability and utility of the Ni–Au NCs in the detection of biomolecules, explosives, and an explosive surrogate at very low concentrations have been demonstrated using Raman spectroscopy and microscopy. Synthesis of such inexpensive, free standing, recyclable, large area SERS substrates by a fast chemistry without the aid of templates or surfactants is advantageous for developing applications.

2. Experimental

2.1. Materials

$NiCl_2\cdot 6H_2O$, $HAuCl_4\cdot 2H_2O$, $PdCl_2$, and hydrazine monohydrate were purchased from SD Fine Chemicals, India (AR grade). Hexachloroplatinic acid ($H_2PtCl_6\cdot 6H_2O$), dipicolinic acid (DPA), and 2,4-dinitrotoluene (DNT) were purchased from Sigma Aldrich. Trinitrotoluene (TNT) and hexahydro-1,3,5-triazine (RDX) were gifts from Indira Gandhi Centre for Atomic Research, Kalpakkam, India. All chemicals were used as such without further purification. Triply distilled water was used throughout the experiments.

2.2. Synthesis of nickel nanowires and nanocarpets

Ni NWs were synthesized by the reduction of nickel chloride in water using concentrated aqueous hydrazine hydrate (HyH) solution as the reducing agent. In a typical synthesis, 1 mL of 250 mM aqueous solution of nickel chloride was added to 9 mL of water at 80 °C to get 25 mM solution of Ni^{2+}. After about one minute, 1 mL of HyH solution was added drop-wise into the solution. No stirring was done during this process. After the addition of HyH, NCs were formed gradually inside the wall of the glass beaker as a silverish film after 5 min. These NCs measuring an area of $\sim$5 cm^2 were then peeled carefully off the beaker. Ni NWs were formed simultaneously inside the solution as a black network-like residue, which was separated by forceps. The NCs and NWs were washed carefully with distilled water and subsequently with alcohol, to remove excess of hydrazine and the other unreacted ions. The methodology could be scaled to get larger quantities of these materials of the order of grams.

2.3. Making of hybrid Ni nanotubes and wires

About 4 mg of the Ni NWs, synthesized as per the above procedure, were immersed inside 500 μL of 10 mM $HAuCl_4$ or H_2PdCl_4 solution in a vial. This solution was shaken gently for 5 min. After that, as formed Ni–Au and Ni–Pd nanotubes were separated out from the solution using a bar magnet. They were then washed carefully with distilled water and subsequently with alcohol, to remove unreacted ions.

In order to make hybrid Ni–Ag and Ni–Pt NWs the aforementioned experiment was conducted using 500 μL of 25 mM H_2PtCl_6 or $AgNO_3$ in place of Au and Pd precursors.

2.4. Ni–Au nanocarpets

Thin films of nickel NCs (4 mg, $\sim$2 cm^2) were immersed inside 500 μL of 10 mM of $HAuCl_4$ in a vial for about 5 min. A visible change from silverish to light brown color indicates the formation of Ni–Au NCs. The Ni–Au NCs were separated out carefully from the solution using forceps, washed with distilled water and subsequently with alcohol and dried. This material was later used for SERS measurements.

In all the abovementioned cases of synthesis of hybrid nanostructures, varying quantities of metal ions were added to the Ni nanostructures to deposit the required amount of metals on them.

3. Instrumentation

Scanning electron microscopy (SEM) imaging and energy dispersive analysis of X-ray (EDAX) studies were done with a FEI QUANTA-200 scanning electron microscope. Raman measurements were done with a WiTec GmbH, Alpha-SNOM CRM 300 instrument having a 633 nm laser with a maximum power of 35 mW. During the Raman measurements, the laser power has been adjusted so as to get a good Raman spectrum. The material was carefully transferred onto a cover glass, and required amounts of analyte solution of finite concentrations were mixed with it. It was then mounted onto the sample stage of the Raman spectrometer. For the SERS measurements, the backscattered light was collected using a 60× liquid immersion objective at an integration time of 1 s. For Raman imaging of Ni–Au nanotubes and Ni–Au NC, the backscattered light was collected using 100× and 20× objectives, respectively, at an integration time of 50 ms. A super notch filter placed in the path of the signal effectively cuts off the excitation radiation. The signal was then dispersed using a 600 grooves per mm grating, and the dispersed light was collected by a Peltier cooled charge coupled device (CCD). Raman enhancement factors were calculated as discussed in earlier reports.[32] XPS measurements were done with an Omicron ESCA Probe spectrometer with unmonochromatized Al Kα X-rays ($h\nu = 1486.6$ eV).

4. Results and discussion

Highly thorny NWs and NCs of Ni were synthesized by following the procedure mentioned in the Experimental section and their morphology was studied using SEM. The NCs were separated as thin films which were several centimetres in length and width (Fig. 1). The surface of the NCs attached onto the wall of the glass beaker appeared silverish and was relatively smooth in appearance (photograph is given in Fig. 6). The other side of the NC which was not attached to the glass wall (in contact with the solution) was highly thorny in nature and appeared black (photograph in Fig. 6). The thorns, which were projecting

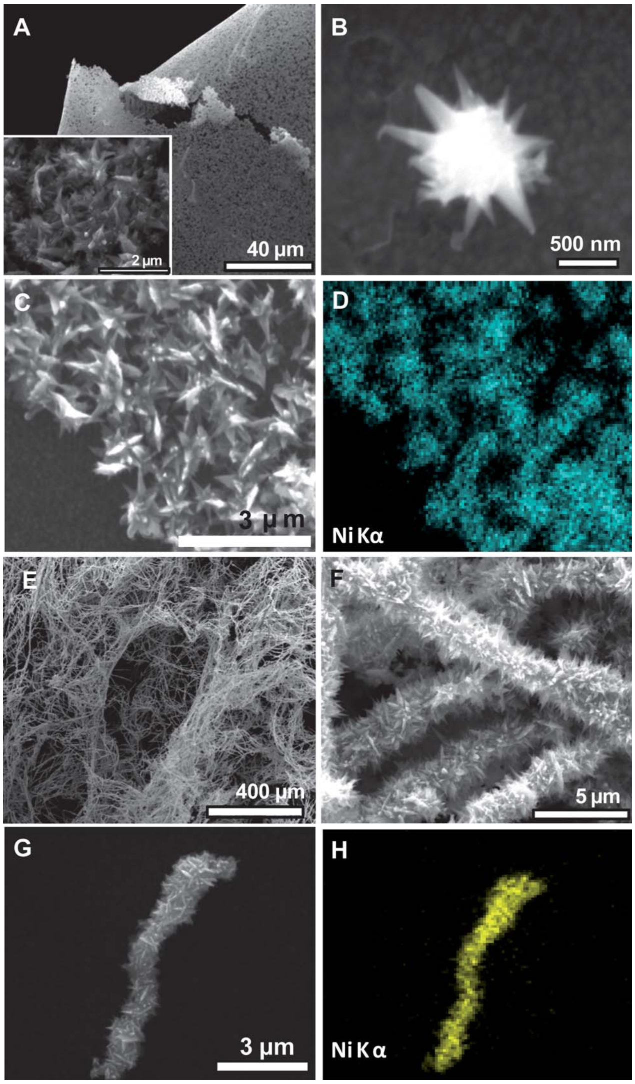

Fig. 1 SEM image of Ni NC (A) and a single nanoflower (B). Inset of (A) is an enlarged view of the Ni NC showing the presence of thorny projections. (C) and (D) are the SEM and corresponding Ni Kα-based EDAX images of Ni NCs. (E) and (F) are the SEM images of thorny Ni NWs taken at various magnifications. (G) and (H) are the SEM and corresponding EDAX images of Ni NWs.

outward from the surface (the inset of Fig. 1A), gave a carpet-like appearance to these films. SEM analysis revealed that these NCs were formed by the self-assembly of several flower-shaped Ni NPs of around 1 µm size, as shown in Fig. 1B.

Since the constituent nanoflowers were not packed densely, the NC appeared highly porous in nature (Fig. 1A). The chemical composition of the Ni NCs was characterized using EDAX (Fig. 1C and D). They are mainly composed of Ni along with some amount of oxygen, probably formed due to the surface oxidation of Ni (ESI, Fig. S1†). While carpets were formed as films, Ni NWs 2 µm in diameter and length up to several hundred microns (Fig. 1E and F) were formed in the solution as a black mass within 10 min. These were separated from the solution using forceps. Closer examination revealed that these wires were highly anisotropic, constructed with a large number of thorns with a length of 100–300 nm (Fig. 1F). The NWs were highly stable. Even long time (30 min) ultrasonication could not break them, indicating that the thorn-like building blocks had fused together.

The chemical composition of the NW was examined using EDAX (Fig. 1G and H). In addition to nickel, small amounts of oxygen were also present which might be attributed to the surface oxidation of nickel due to the high reactivity of elemental nickel (ESI, Fig. S2†).

The temperature dependence of the surface structure of these NWs has been studied. We found that the surface of the thorny NWs (Fig. 2A) became fairly smooth when the reaction was carried out at elevated temperatures in ethylene glycol as solvent. The synthesis yielded Ni NWs with an average diameter of ~200 nm in very large quantity without any other NPs of different morphology (Fig. 2A and B). The amount of HyH also plays an important role in determining the surface structure of the NW. At low concentration of HyH (100 µL), sphere-like NPs were formed and NWs were not seen (Fig. 2C). Some of these particles tend to self-assemble to form chain-like structures. As the amount of HyH increases (500 µL), an increase in the number of thorns present on the NW surface was observed (Fig. 2D). Further increase of the reducing agent (1 mL) resulted in the formation of highly thorny Ni NWs (Fig. 2E). The number of thorns was found to decrease when excess amount of reducing agent (5 mL) was added (Fig. 2F). At an elevated temperature and at a high concentration of the reducing agent, reduction of

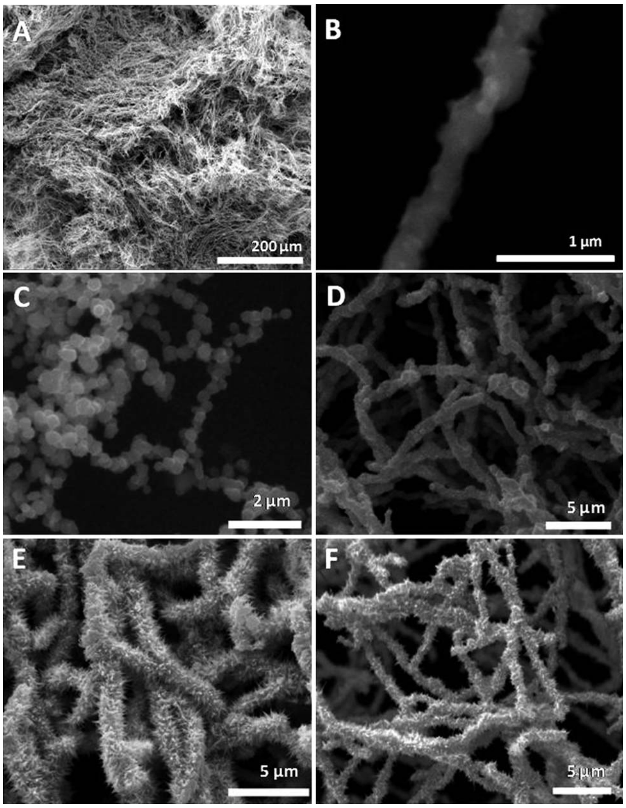

Fig. 2 Large area (A) and enlarged (B) SEM images of the Ni NWs formed when ethylene glycol was used as a solvent at 130 °C. (C)–(F) are the SEM images of the nanostructures synthesized using various amounts of HyH such as 0.1, 0.5, 1.0, and 5.0 mL, respectively, keeping other parameters the same.

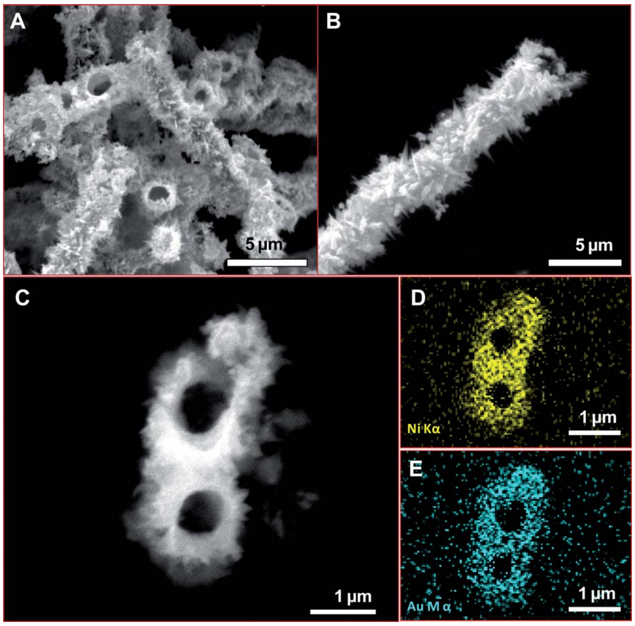

Fig. 3 SEM images (A–C) of the sample $\mathbf{A_1}$ taken in various magnifications. (D) and (E) are Ni Kα and Au Mα based EDAX maps of the tip of a nanotube shown in (C).

metal ions may happen at a faster rate, resulting in the formation of a smooth surface. Though thorny NPs and NWs of Ni were seen earlier with the assistance of a surfactant and an external magnetic field,[33–38] our synthetic protocol is very simple, which does not require any surfactant or magnetic field. It is proposed that at the initial stage of the reaction, $NiCl_2$ undergoes complexation with HyH. In the subsequent step, this complex is reduced by excess HyH to form smaller Ni nuclei. These nanocrystals could serve as seeds as well as provide catalytic surfaces for further growth of larger particles. Further reduction of Ni ions happens at these seed surfaces in all directions to form spherical NPs.

Since the circumferential edges have higher free energies,[39] further reduction may preferentially occur at these relatively more active sites which lead to the formation of a spiky surface. The high reducing capacity of HyH at higher temperatures[40] enhances the reduction rate of Ni ions. At elevated temperatures, these spiky nanospheres may tend to join each other to reduce surface energy. Subsequently, these nickel crystals would connect to form hierarchical nickel NWs. Reduction in the surface energy by the elimination of the interface during this process may facilitate NW formation. In the following steps, further deposition of Ni ions continues at these spear-like nickel stems, which grow longer toward different directions until all of the nickel ions are consumed. Continuous heating of the reaction mixture for about 30 min resulted in the formation of branched NWs (ESI, Fig. S3†). In the case of NC formation, the assembly of smaller nanoflowers may happen laterally in all directions which results in sheet-like structures.

4.1. Galvanic replacement reaction

Since nickel has a relatively lower reduction potential than noble metals, the Ni NCs and NWs have been used as sacrificial templates for the galvanic displacement reaction[23–26] to make

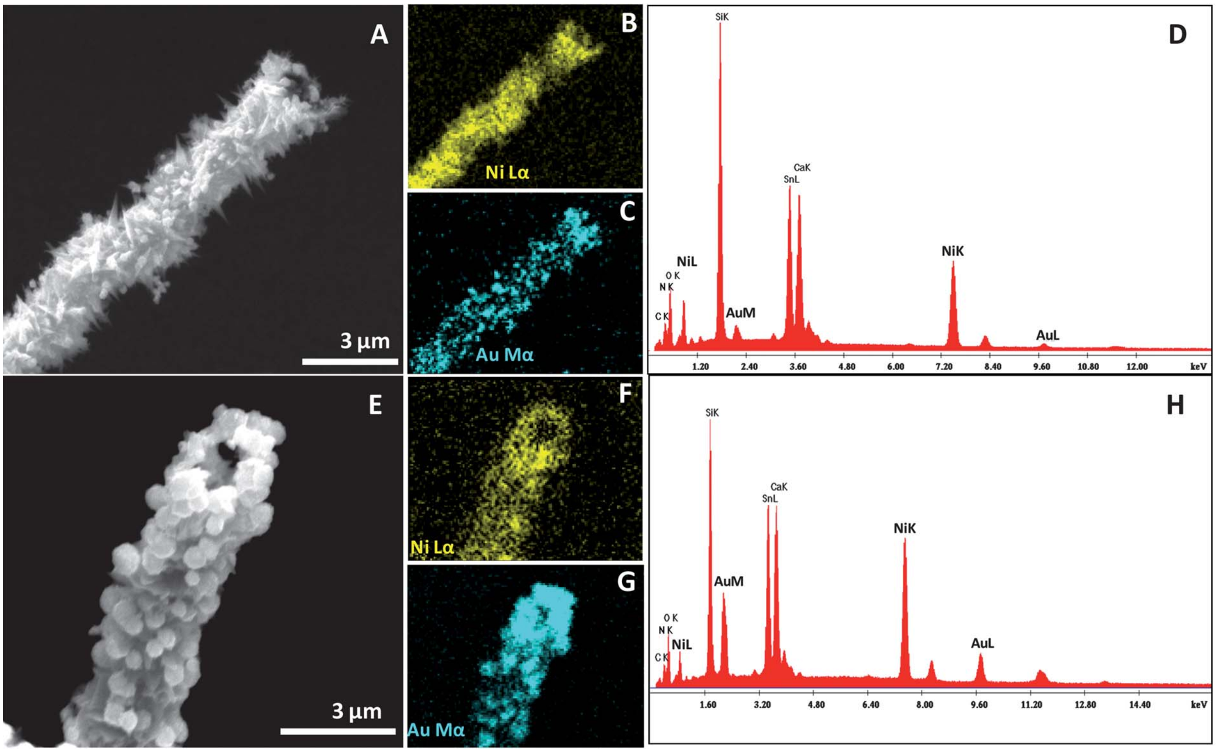

Fig. 4 (A) and (E) are the SEM images of the sample $\mathbf{A_1}$ and $\mathbf{A_2}$, respectively. Corresponding EDAX images and spectra are also given. The elements Ca, Sn and Si are due to the ITO conducting glass substrate used.

hybrid systems with Au, Ag, Pt, and Pd. In such experiments, the metal nanocrystal will get oxidized by the noble metal ion which has a more positive reduction potential. In the case of Ni NWs, after the addition of Au^{3+}, interestingly we found that the NWs get converted to nanotubes. The resultant Ni–Au nanotubes were characterized using SEM (Fig. 3). Almost all the NWs underwent the galvanic displacement reaction and converted to nanotubes (Fig. 3A). Fig. 3B reveals the tubular nature of these hybrid nanomaterials. From the SEM images, it is clear that the tips of the NWs undergo reaction easily resulting in nanotubes with holes, mostly at the center of the tip which could be attributed to the high reactivity of the tip of such one dimensional NWs.[41] After the addition of Au^{3+} into the Ni NWs, the displacement reaction happens at sites of relatively high surface energies such as point defects, stacking fault, steps, *etc.*[42] During the reaction, Ni atoms diffused to the surface of the NCs and Au atoms diffused into the structure. More Ni atoms on the NW surface will get displaced by Au atoms as etching creates Ni surfaces with higher surface energies. At the same time, epitaxial growth of Au results in the formation of thin films at the surface of Ni NWs and subsequent etching will happen at the interior of the NWs, newly formed high energy Ni surfaces are now abundant. This could lead to the formation of nanotubes. The Kirkendall effect[43] is also expected to play a significant role in the formation of such nanotubes.

The chemical composition of these hybrid nanotubes was further confirmed by EDAX (Fig. 3C–E), which shows the presence of Ni and Au. Well-defined nanotubes as shown in Fig. 3 were obtained in 5 min when 500 µL of 10 mM of Au^{3+} was added into 4 mg of the Ni NWs (we refer to this sample as $\mathbf{A_1}$). Upon increasing the concentration of Au^{3+} from 10 mM to 25 mM (referred to as $\mathbf{A_2}$), a greater amount of gold was deposited onto the Ni NWs after 5 min and the NW surface was decorated with nearly spherical gold nanobeads.

SEM images and corresponding EDAX data showing the variation in the elemental compositions of the Ni–Au nanotubes with increasing concentration of Au^{3+} are given in Fig. 4. Ni–Au nanotubes formed after 5 min of addition of 500 µL of 10, 15, and 25 mM of Au^{3+} into 4 mg of Ni NWs are shown in ESI (Fig. S4†). As the reaction proceeds, a greater amount of Au was deposited onto the NW surface.

A similar approach was followed to make various hybrid nanomaterials such as Ni–Pd nanotubes, Ni–Pt, and Ni–Ag NWs. For Pd, by the addition of 500 µL of 25 mM Pd^{2+} solution, the Ni NWs were converted to Ni–Pd nanotubes as in the case of Ni–Au nanotubes (Fig. 5A and B) whereas the nanotube formation was not observed for the same amount of Ag or Pt ions. At this particular concentration of metal ions, instead of forming nanotubes, Ag and Pt got deposited onto the Ni NW surface to form hybrid Ni–Ag and Ni–Pt NWs, respectively. The

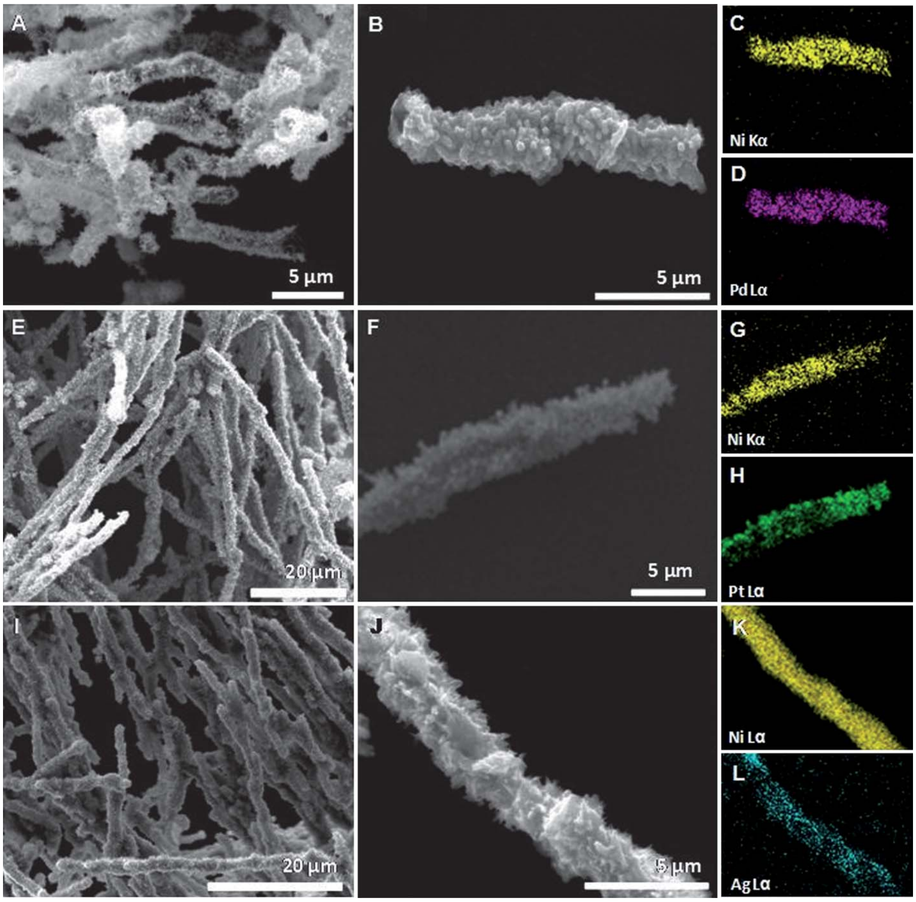

Fig. 5 (A), (E), and (I) are large area SEM images of Ni–Pd nanotubes, and Ni–Pt and Ni–Ag NWs, respectively. Single particle SEM images (B, F, and J) and corresponding EDAX images (C, D, G, H, K, and L) of these nanostructures are also given.

large area and corresponding single particle SEM images of Ni–Pd nanotubes as well as Ni–Pt and Ni–Ag NWs are given in Fig. 5. The chemical composition of these hybrid nanostructures was characterized using EDAX (Fig. 5C, D, G, H, K, and L).

We also made bimetallic Ni–Au NCs *via* the galvanic displacement reaction by the addition of Au^{3+} into the Ni NCs. By the addition of 500 μL of 10 mM of Au^{3+} into 4 mg of Ni NCs, we could make ~4 mg of Ni–Au bimetallic NCs (this sample is referred to as $\mathbf{B_1}$ with 2 cm^2 surface area, having almost the same morphology as the parent Ni NCs (Fig. 6E)). After the deposition of Au, the sharpness of the thorns reduced slightly compared to that of Ni NCs (Fig. 6D). The inset of Fig. 6E shows a magnified SEM image of the bimetallic NCs in which the thorns are projecting outward from the surface. Photographs of a large-area Ni NC before and after treatment with Au^{3+} solution are shown in Fig. 6A–C.

As all the Au^{3+} added were not reacted with Ni atoms in the replacement reaction, a significant amount of Ni remained inside the nanocarpet (see ESI, Fig. S5†). As the reactivity at the tip of each thorn is high, the displacement reaction happened to a greater extent at the tip and a greater amount of Au was deposited at the tip. EDAX data suggested that the ratio of atomic percentage of Au and Ni in $\mathbf{B_1}$ is ~1 : 4 (ESI, Fig. S5†). A greater amount of Au was deposited by increasing the concentration of Au^{3+} from 10 mM to 15 mM. The nanothorns present on the NCs were converted to spherical NPs with roughened surfaces of around 500 nm diameter, and the carpet was looking like a film made by the assembly of spheres as shown in Fig. 6F. Again when the concentration of Au increased to 25 mM (referred to as $\mathbf{B_2}$), a greater amount of Au^{3+} was deposited and the size of the spheres increased from ~500 nm to ~3 μm (Fig. 6G). Even after the galvanic displacement reaction, these

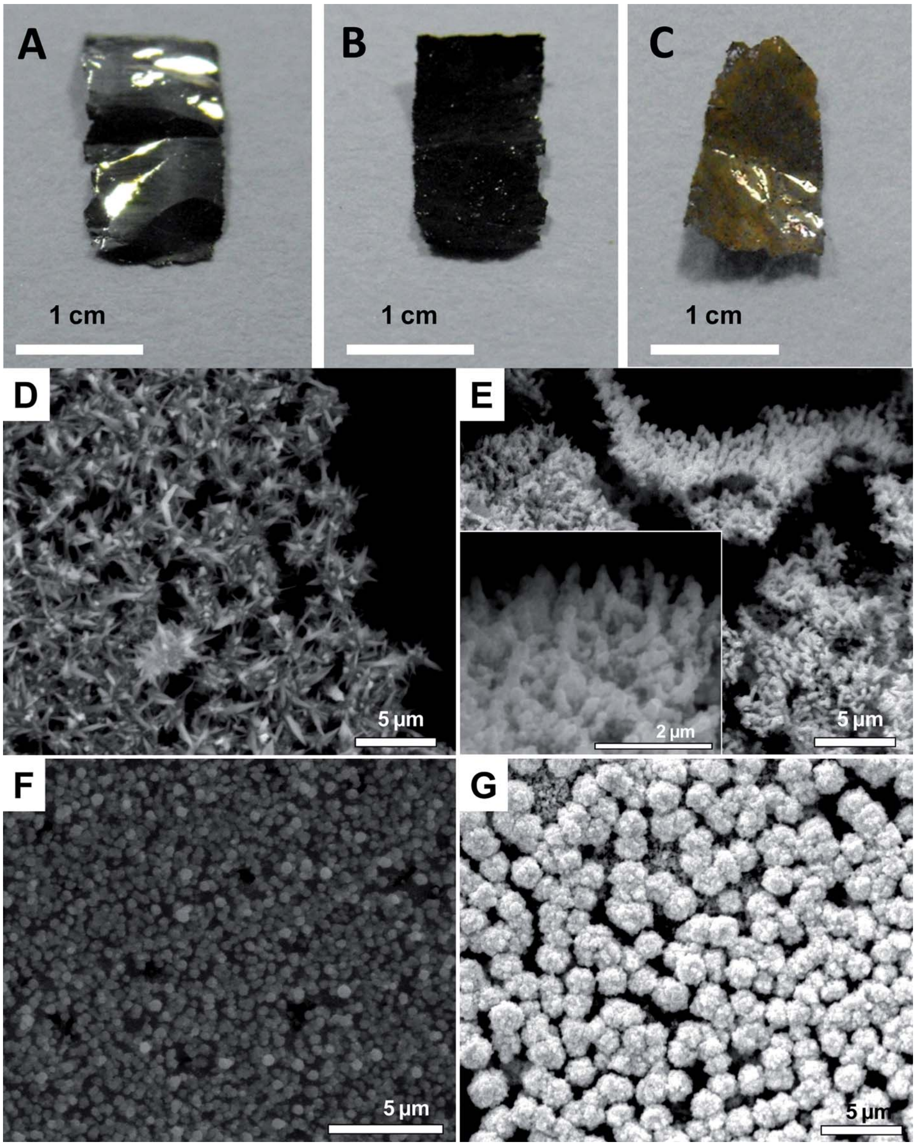

Fig. 6 Photographs of the Ni NC before (A (the side attached to the glass beaker is facing the viewer) and B (the side in contact with the solution)) and after (C) treatment with Au^{3+} solution. (D) SEM image of Ni NC showing a large number of spiky projections before the galvanic displacement reaction. (E)–(G) are Ni–Au NCs formed by the addition of 500 μL of 10, 15, and 25 mM of Au^{3+}, respectively, into 4 mg of Ni NCs.

NCs were not completely fragmented or disassembled, but existed as a film.

The chemical compositions of NCs and NWs of Ni and hybrid Ni–Au NCs and nanotubes were characterized by using X-ray photoelectron spectroscopy (XPS). The wide scan XPS spectra of NCs and NWs of Ni and bimetallic Ni–Au NCs and nanotubes are given in Fig. 7A. The enlarged scan of Ni 2p of Ni NCs and NWs showed $2p_{3/2}$ at ~855.5 eV and $2p_{1/2}$ at ~873.5 eV (Fig. 7B). At the same time, the Ni 2p region of Ni–Au NCs showed $2p_{3/2}$ at ~855.3 eV and $2p_{1/2}$ at ~873.3 eV (Fig. 7C). In the case of Ni–Au nanotubes, Ni $2p_{3/2}$ and $2p_{1/2}$ were observed at ~855.4 eV and at ~873.1 eV, respectively. The observed shift in the Ni 2p peaks in all the above mentioned cases toward the higher binding energy region compared to Ni(0) (852.6 eV) can be due to the possible existence of Ni^{2+} in the form of oxide coating on the surface of these Ni nanosurfaces. The presence of satellite peaks found in the high-binding energy region confirms the existence of Ni in its divalent state.[44–46] Poor intensity of the satellite features indicates that the extent of surface oxidation at the surface of Ni nanostructures is small. The O 1s peaks found around 531.4 eV in all the cases (see ESI, Fig. S6†) again confirm the presence of O^{2-}. The 4f region of Au in Ni–Au NCs and nanotubes is given in Fig. 7D. The spectra showed the presence of Au $4f_{7/2}$ and Au $4f_{5/2}$ peaks at ~84.1 and ~87.8 eV, respectively, confirming the existence of gold in its metallic form, due to galvanic exchange.

4.2. SERS measurements

Noble metal NPs with sharp edges and corners exhibit an enhanced electric field around these locations capable of enhancing the intensities of Raman signals of molecules present there.[4,8,9,47,48] In our case, these spiky Ni–Au bimetallic nanotubes and NCs with highly roughened surfaces, devoid of any surfactants or organic species, exhibited very good SERS activity. The SERS activity of the nanomaterials has been studied using crystal violet (CV) as the analyte. For the SERS study, we selected four different substrates such as Ni–Au nanotubes (**A_1** and **A_2**) and Ni–Au NCs (**B_1** and **B_2**).

Samples **A_1** and **B_1** corresponding to reaction with 10 mM Au^{3+} showed much better SERS activity compared to the other two using a higher concentration of Au^{3+}. The SERS spectra collected from various nanomaterials and corresponding SEM images are given in Fig. 8. From a detailed study, we found that the sample **B_1** can detect CV up to a concentration of 10^{-11} M (ESI, Fig. S7†) with an enhancement factor[49,50] of the order of ~10^{10}. Even at a concentration of 10^{-11} M, we got characteristic Raman features of CV adsorbed on Ni–Au NC. The high SERS activity of Ni–Au NCs and nanotubes can be attributed to the presence of the spiky tips as well as highly corrugated surfaces acting as hot spots. Comparatively less SERS activity of the other two systems (**A_2** and **B_2**) can be due to the absence of the sharp thorns (due to the deposition of a greater amount of Au^{3+}, spiky thorns were converted into nearly spherical particles). However, they also showed SERS activity with an EF of the order of ~10^7, attributed to the presence of a highly roughened surface. Apart from this, the junction between the adjacent nanospheres in the self-assembled film or wires can also act as hot spots, capable of enhancing the intensity of Raman signals. Recently, Mirkin *et al.* have shown that very long range SERS is possible in a nickel NW separated by a pair of gold nanodisks by the excitation of the surface-plasmon resonance from the gold nanodisk pair.[51] A Raman image of a Ni–Au nanotube created by integrating the spectral intensities of adsorbed CV molecules

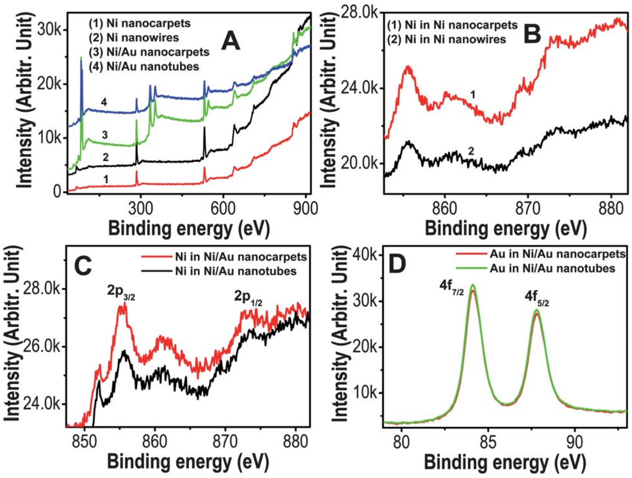

Fig. 7 (A) Wide scan XPS spectra of NCs and NWs of Ni and bimetallic Ni–Au NCs and nanotubes. (B) The Ni 2p region of Ni NCs and NWs. (C) The Ni 2p region of Ni–Au NCs and nanotubes. (D) The Au 4f region of Ni–Au NCs and nanotubes.

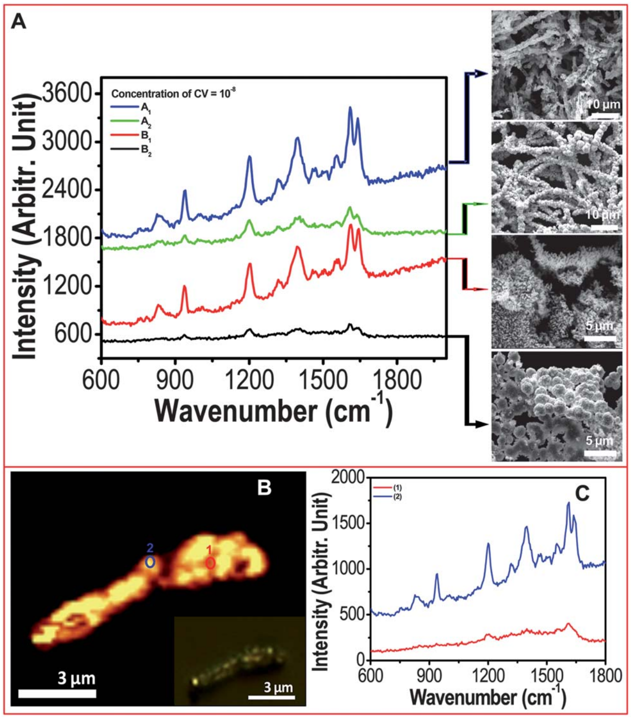

Fig. 8 (A) Raman spectra collected from **A_1**, **A_2**, **B_1**, and **B_2** upon exposure to 10^{-8} M CV. Representative large area SEM images of each Ni–Au nanosubstrate are shown along with the spectra. (B) Raman image of a Ni–Au nanotube created by integrating the spectral intensities of adsorbed CV between 1200 and 1700 cm^{-1}. The inset shows the optical image of the nanotube used for Raman imaging. (C) Raman spectra collected the two regions marked in the Raman image shown in (B).

(10^{-8} M) between the 1200 and 1700 cm^{-1} window is shown in Fig. 8B. From the Raman image, it is clear that the enhancement of the Raman features is not uniform throughout the nanotubes.

The spectra collected from various regions of the nanotube showed varying intensities at different regions (Fig. 8C). This can be due to the uneven distribution of gold at the surface of the nanotubes. The more SERS active Au rich region (spot 2) showed higher intensities compared to the Ni rich areas (spot 1) which is not as good as Au in terms of its SERS activity. This result confirms that the deposition of Au onto the Ni NW during the galvanic displacement reaction is not uniform; hence there will be slight differences in the intensities of SERS signal at different points.

Taking advantage of the high SERS activity of sample **B$_1$**, we demonstrated the utility of this material as an SERS substrate for the detection of certain analytes such as DPA, a molecule which constitutes 5 to 15% of the dry weight of the bacterial spore of *Bacillus anthracis*, the explosives TNT and RDX and an explosive surrogate, DNT. In our study, first we took the Ni–Au NCs on a glass substrate and 20 μL of the analyte solutions of different concentrations were drop-casted. The substrate was subjected to an SERS test in ambient air. The back-scattered light was collected using a 60× liquid immersion objective with an integration time of 1 s. The enhancement factors (EFs) were calculated in all the cases for a lower detection limit. We could detect the characteristic Raman features of DNT and TNT up to a concentration of 10^{-7} M (EF $\approx 10^6$) (Fig. 9). In the case of DPA, the detection limit was 10^{-8} M (EF $\approx 10^7$). We could get distinct Raman features up to 10^{-6} M (EF $\approx 10^5$) for RDX. In all the cases, the resulting Raman features were comparable with the standard solid samples. The multi-analyte detection capability of our SERS substrate makes it highly promising for defense- or diagnostics-related applications.

4.3. Reusability of Ni nanocarpet

Further, to demonstrate the reusability of the Ni–Au NCs after each Raman measurement, the substrate was subjected to a sequence of cleaning procedures. Each cycle of cleaning includes washing of the substrate with deionized water (after the SERS measurements) followed by gentle sonication with acetone for about 1 min. The substrate was then kept at 300 °C for 30 min in a furnace to remove volatile organic components and the resulting substrate was used for further SERS measurements. Even after heat treatment, the surface morphology of the NCs remained almost unchanged. Fig. 10A and B show the SEM

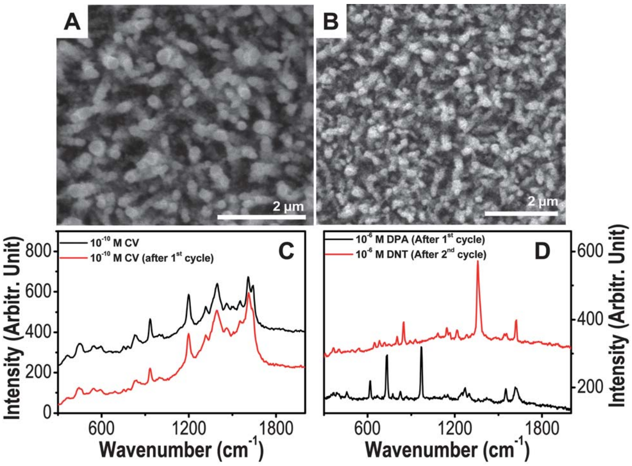

Fig. 10 SEM images of the sample **B$_1$** before (A) and after (B) the first cycle of cleaning. (C) Raman spectra of 10^{-10} M of CV collected from **B$_1$** before (black trace) and after 1st cycle of cleaning (red trace). (D) Raman spectra of 10^{-6} M of DPA and DNT adsorbed on **B$_1$** after 1st and 2nd cycles of cleaning.

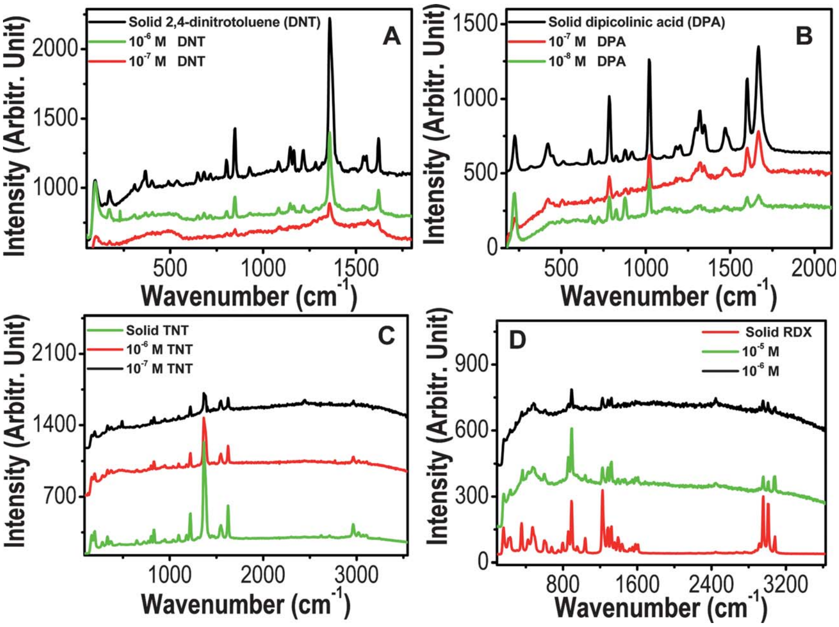

Fig. 9 Raman spectra of DNT (A), DPA (B), TNT (C) and RDX (D) solutions of various concentrations adsorbed on **B$_1$**. The traces are given in the same intensity scale, but shifted vertically for clarity.

images of the Ni–Au NCs before and after heat treatment. The resultant substrate was devoid of any Raman features of CV (ESI, Fig. S8†). Even though there is a possibility of oxidation of Ni during heat treatment, it did not affect the SERS activity of the Ni–Au NC as gold is mainly responsible for the SERS enhancement which was quite stable at that temperature. However, it is to be noted that the adsorption strength of the analyte may also play a role in the reusability of this material.

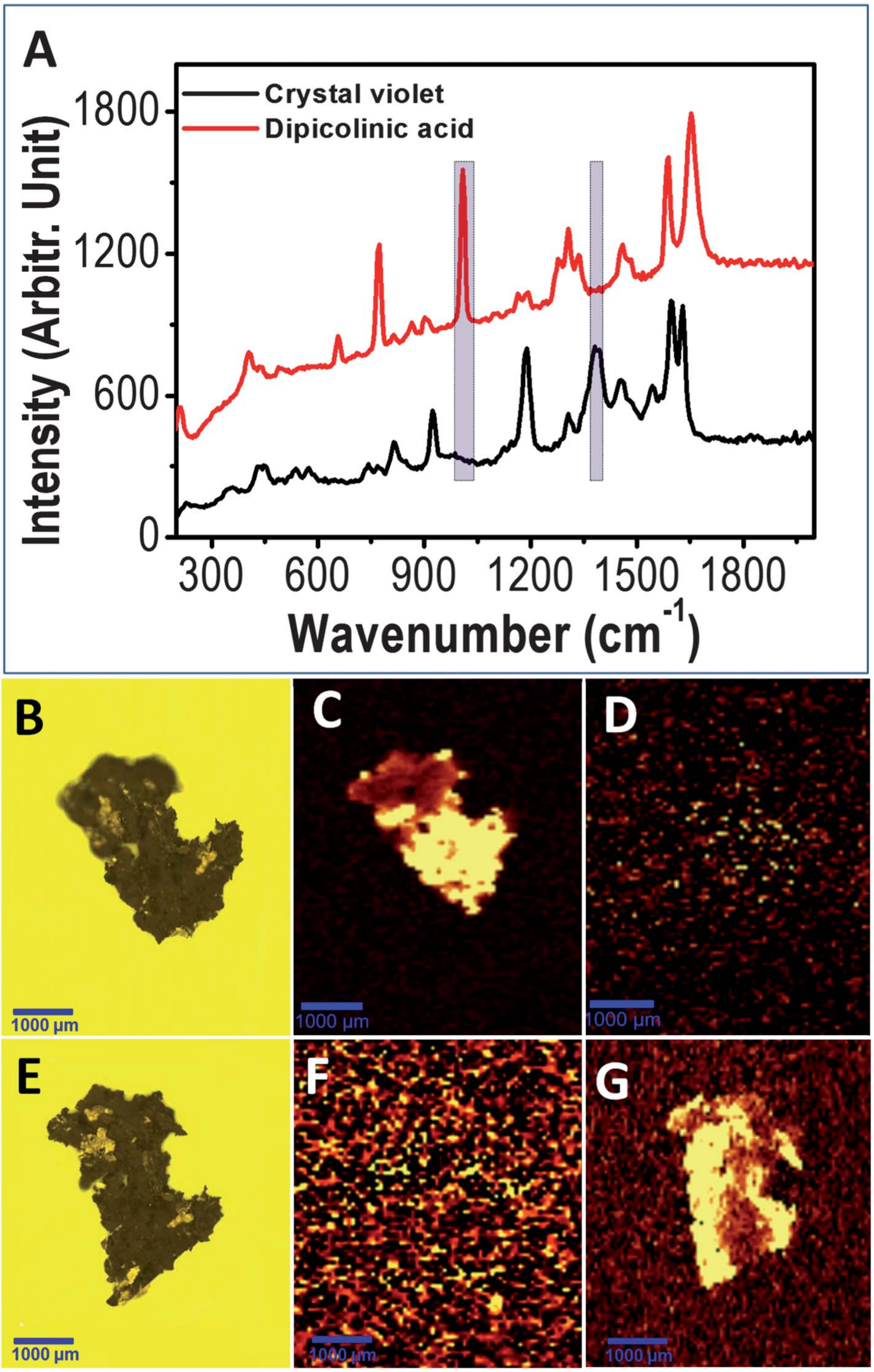

Fig. 11 (A) Raman spectrum of 10^{-6} M of CV (black trace) collected from $\mathbf{B_1}$ before the 1st cycle of cleaning. Red trace shows the Raman spectrum of 10^{-6} M of DPA adsorbed on the same sample $\mathbf{B_1}$ after the 1st cycle of cleaning. (B) and (E) are the optical images of $\mathbf{B_1}$ before and after the 1st cycle of cleaning, respectively. (C) and (D) are the Raman images of $\mathbf{B_1}$ acquired by collecting the Raman intensities of the peaks in the range of 1375–1382 and 995–1002 cm^{-1}, respectively. 10^{-6} M of CV was used as analyte for the Raman imaging. (F) and (G) are the Raman images of $\mathbf{B_1}$ (after the first cycle of cleaning) acquired by collecting the Raman intensities of the peaks in the range of 1375–1382 and 995–1002 cm^{-1}, respectively. Here, DPA (10^{-6} M) was used as analyte for the Raman imaging.

Some molecules may have to be heated well above 300 °C for complete desorption. So there is a chance of structural transformation of the NCs which may affect its sensitivity.

After the first cycle of cleaning, the same substrate was used for SERS measurements. The substrate showed similar Raman spectra of CV at a concentration of 10^{-10} M, with its characteristic Raman features with almost the same intensity (Fig. 10C). The distance between the substrate and the microscope objective was adjusted so as to get maximum Raman intensity. We checked the reusability of the substrate by measuring the Raman spectra after subsequent washing and cleaning processes many times. After each cycle of cleaning, we verified the efficiency of the substrate by collecting the spectra of adsorbed CV. The results obtained using recycled substrates were comparable to the Raman spectra recorded using fresh substrates. The Raman spectra of 10^{-9} M CV collected from the Ni–Au NC after it was subjected for five cycles of cleaning showed almost all the characteristic features of CV (ESI, Fig. S9†). The SERS sensitivity was found to be decreased upon further use of the same substrate.

To test the sensitivity of the reprocessed substrates, we conducted the same procedure with different molecules, one after the other on the same substrate. For that, first we used the sample $\mathbf{B_1}$ after the first cycle of the cleaning process (previously used for the SERS measurement with CV solution) and drop casted DPA solution of 10^{-6} M concentration. The spectrum collected showed the Raman features of DPA molecule (Fig. 10D). The same substrate was subjected to a second cycle of the cleaning process and again used for the SERS study with a DNT solution of 10^{-6} M. Using that substrate, we could get the distinct Raman features of DNT (Fig. 10D).

The sensitivity of the recycled Ni–Au NCs towards its SERS activity was further verified by collecting the Raman image of a large area film, before and after recycling, using various analytes such as CV and DPA. We selected two different regions of 1375–1382 and 995–1002 cm^{-1} for imaging due to the reason that CV shows an intense *N*-phenyl stretching[16] band at 1379 cm^{-1}, which is absent in DPA. At the same time, DPA shows an intense symmetric ring breathing mode[52] at 998 cm^{-1} which is almost absent or weak (appears at 992 cm^{-1} as a weak band) in the case of CV. Fig. 11C and D show Raman images of the Ni–Au NC (before recycling) acquired by collecting the Raman intensities of the adsorbed CV in the range of 1375–1382 and 995–1002 cm^{-1}, respectively. The optical image of the Ni–Au NC selected for the Raman imaging is shown in Fig. 11B. The Raman image of the Ni–Au NC in (C) appeared bright and there was no such image in Fig. 11D. After the Raman measurements, we carefully cleaned the substrate without any serious damage to the material, treated it with 10^{-6} M of DPA, and collected the Raman image. In this case, we could get the Raman image using intensities in the range of 995–1002 cm^{-1}. But, there was no such image found for the 1375–1382 cm^{-1} range. This indicates that the adsorbed CV molecules were completely removed from the NC after the first cycle of cleaning. The Raman study shows that we can successfully regenerate the NC substrate without losing its sensitivity after recycling.

5. Conclusions

A facile and cost-effective way to make reusable, highly SERS active, and free-standing large area nanocarpets, extending over cm^2 area, has been developed through a galvanic replacement reaction, starting from prefabricated Ni NCs. Using the same approach we made highly SERS active nanotubes from Ni NWs. We demonstrated the viability of our method to make several hybrid nanoystems such as Ni–Pd nanotubes and Ni–Pt and Ni–Ag NWs in an easy manner by following the same procedure. The high SERS activity of these hybrid materials has been utilized to detect molecules such as dipicolinic acid, dinitrotoluene, trinitrotoluene, and RDX at very low concentrations. We verified that the Ni–Au NC can be reused multiple times as SERS substrates without significant loss of its activity. Compared with other conventional SERS substrates, reusable and highly SERS active, large area Ni–Au NCs made by a cost-effective method may be a perfect choice for making large area sensors in many practical applications.

Acknowledgements

We thank the Department of Science and Technology, Government of India for constantly supporting our research program on nanomaterials.

References

1 M. E. Stewart, C. R. Anderton, L. B. Thompson, J. Maria, S. K. Gray, J. A. Rogers and R. G. Nuzzo, *Chem. Rev.*, 2008, **108**, 494–521.

2 S. R. Nicewarner-Pena, R. G. Freeman, B. D. Reiss, L. He, D. J. Pena, I. D. Walton, R. Cromer, C. D. Keating and M. J. Natan, *Science*, 2001, **294**, 137–141.

3 R. Narayanan and M. A. El-Sayed, *J. Am. Chem. Soc.*, 2004, **126**, 7194–7195.

4 J. P. Xie, Q. B. Zhang, J. Y. Lee and D. I. C. Wang, *ACS Nano*, 2008, **2**, 2473–2480.

5 C. Wang, Y. Chen, T. Wang, Z. Ma and Z. Su, *Adv. Funct. Mater.*, 2008, **18**, 355–361.

6 J. B. Jackson, S. L. Westcott, L. R. Hirsch, J. L. West and N. J. Halas, *Appl. Phys. Lett.*, 2003, **82**, 257–259.

7 M. J. Banholzer, J. E. Millstone, L. Qin and C. A. Mirkin, *Chem. Soc. Rev.*, 2008, **37**, 885–897.

8 C. G. Khoury and T. Vo-Dinh, *J. Phys. Chem. C*, 2008, **112**, 18849–18859.

9 P. R. Sajanlal and T. Pradeep, *Nano Res.*, 2009, **2**, 306–320.

10 L. A. Lyon, C. D. Keating, A. P. Fox, B. E. Baker, L. He, S. R. Nicewarner, S. P. Mulvaney and M. J. Natan, *Anal. Chem.*, 1998, **70**, 341R–361R.

11 P. R. Sajanlal and T. Pradeep, *Adv. Mater.*, 2008, **20**, 980–983.

12 J. E. Millstone, S. Park, K. L. Shuford, L. Qin, G. C. Schatz and C. A. Mirkin, *J. Am. Chem. Soc.*, 2005, **127**, 5312–5313.

13 F. Hao, C. L. Nehl, J. H. Hafner and P. Nordlander, *Nano Lett.*, 2007, **7**, 729–732.

14 P. R. Sajanlal and T. Pradeep, *Langmuir*, 2010, **26**, 8901–8907.

15 L. J. Sherry, S.-H. Chang, G. C. Schatz, D. R. P. Van, B. J. Wiley and Y. Xia, *Nano Lett.*, 2005, **5**, 2034–2038.

16 E. S. Shibu, K. Kimura and T. Pradeep, *Chem. Mater.*, 2009, **21**, 3773–3781.

17 E. S. Shibu, J. Cyriac, T. Pradeep and J. Chakrabarti, *Nanoscale*, 2011, **3**, 1066–1072.

18 P. R. Sajanlal, C. Subramaniam, P. Sasanpour, B. Rashidian and T. Pradeep, *J. Mater. Chem.*, 2010, **20**, 2108.

19 D. P. Fromm, A. Sundaramurthy, P. J. Schuck, G. Kino and W. E. Moerner, *Nano Lett.*, 2004, **4**, 957–961.

20 L. Chen, X. Han, J. Yang, J. Zhou, W. Song, B. Zhao, W. Xu and Y. Ozaki, *J. Colloid Interface Sci.*, 2011, **360**, 482–487.

21 O. Peron, E. Rinnert, T. Toury, M. Lamy de la Chapelle and C. Compere, *Analyst*, 2011, **136**, 1018–1022.

22 J. A. Dieringer, A. D. McFarland, N. C. Shah, D. A. Stuart, A. V. Whitney, C. R. Yonzon, M. A. Young, X. Zhang and D. R. P. Van, *Faraday Discuss.*, 2006, **132**, 9–26.

23 L. Au, X. Lu and Y. Xia, *Adv. Mater.*, 2008, **20**, 2517–2522.
24 X. Lu, H.-Y. Tuan, J. Chen, Z.-Y. Li, B. A. Korgel and Y. Xia, *J. Am. Chem. Soc.*, 2007, **129**, 1733–1742.
25 L. Au, Y. Chen, F. Zhou, P. H. C. Camargo, B. Lim, Z.-Y. Li, D. S. Ginger and Y. Xia, *Nano Res.*, 2008, **1**, 441–449.
26 S. E. Skrabalak, J. Chen, Y. Sun, X. Lu, L. Au, C. M. Cobley and Y. Xia, *Acc. Chem. Res.*, 2008, **41**, 1587–1595.
27 A. J. Chung, Y. S. Huh and D. Erickson, *Nanoscale*, 2011, **3**, 2903–2908.
28 Y. Lai, W. Pan, D. Zhang and J. Zhan, *Nanoscale*, 2011, **3**, 2134–2137.
29 V. V. Hardikar and E. Matijevic, *J. Colloid Interface Sci.*, 2000, **221**, 133–136.
30 T. Bala, S. D. Bhame, P. A. Joy, B. L. V. Prasad and M. Sastry, *J. Mater. Chem.*, 2004, **14**, 2941–2945.
31 T. Bala, S. K. Arumugam, R. Pasricha, B. L. V. Prasad and M. Sastry, *J. Mater. Chem.*, 2004, **14**, 1057–1061.
32 P. R. Sajanlal and T. Pradeep, *J. Nanosci. Nanotechnol.*, 2009, **9**, 5283–5287.
33 M. Zhang, J. Deng, M. Zhang and W. Li, *Chin. J. Catal.*, 2009, **30**, 447–452.
34 D.-P. Wang, D.-B. Sun, H.-Y. Yu and H.-M. Meng, *J. Cryst. Growth*, 2008, **310**, 1195–1201.
35 X. Ni, J. Zhang, Y. Zhang and H. Zheng, *J. Colloid Interface Sci.*, 2007, **307**, 554–558.
36 G. Zhang, T. Zhang, X. Lu, W. Wang, J. Qu and X. Li, *J. Phys. Chem. C*, 2007, **111**, 12663–12668.
37 D. Liu, S. Ren, H. Wu, Q. Zhang and L. Wen, *J. Mater. Sci.*, 2008, **43**, 1974–1978.
38 S. Sarkar, A. K. Sinha, M. Pradhan, M. Basu, Y. Negishi and T. Pal, *J. Phys. Chem. C*, 2011, **115**, 1659–1673.
39 Y. Wang, Q. Zhu and H. Zhang, *Mater. Res. Bull.*, 2007, **42**, 1450–1456.
40 L. Bai, F. Yuan and Q. Tang, *Mater. Lett.*, 2008, **62**, 2267–2270.
41 T. S. Sreeprasad, A. K. Samal and T. Pradeep, *Langmuir*, 2007, **23**, 9463–9471.
42 Y. Sun, *Nanoscale*, 2010, **2**, 1626–1642.
43 H. J. Fan, U. Gösele and M. Zacharias, *Small*, 2007, **3**, 1660–1671.
44 A. F. Carley, S. D. Jackson, J. N. O'Shea and M. W. Roberts, *Phys. Chem. Chem. Phys.*, 2001, **3**, 274–281.
45 P. F. Luo, T. Kuwana, D. K. Paul and P. M. A. Sherwood, *Anal. Chem.*, 1996, **68**, 3330–3337.
46 S. K. Sharma, V. Zaporojtchenko, J. Zekonyte, A. Buettner, S. Deki and F. Faupel, *J. Mater. Sci.*, 2004, **39**, 6291–6297.
47 E. N. Esenturk and W. A. R. Hight, *J. Raman Spectrosc.*, 2009, **40**, 86–91.
48 L. Rodriguez-Lorenzo, R. A. Alvarez-Puebla, I. Pastoriza-Santos, S. Mazzucco, O. Stephan, M. Kociak, L. M. Liz-Marzan and d. A. F. J. Garcia, *J. Am. Chem. Soc.*, 2009, **131**, 4616–4618.
49 (*a*) G. V. P. Kumar, S. Shruthi, B. Vibha, B. A. A. Reddy, T. K. Kundu and C. Narayana, *J. Phys. Chem. C*, 2007, **111**, 4388–4392; (*b*) E. C. Le Ru, E. Blackie, M. Meyer and P. G. Etchegoin, *J. Phys. Chem. C*, 2007, **111**, 13794–13803; (*c*) G. Upender, R. Satyavathi, B. Raju, K. Shadak Alee, D. Narayana Rao and C. Bansal, *Chem. Phys. Lett.*, 2011, **511**, 309–314.
50 K. Kim, H. J. Jang and K. S. Shin, *Analyst*, 2009, **134**, 308–313.
51 W. Wei, S. Li, J. E. Millstone, M. J. Banholzer, X. Chen, X. Xu, G. C. Schatz and C. A. Mirkin, *Angew. Chem., Int. Ed.*, 2009, **48**, 4210–4212.
52 A. A. Kolomenskii and H. A. Schuessler, *Spectrochim. Acta, Part A*, 2005, **61**, 647–651.